Imprint of Accretion Disk-Induced Migration on Gravitational Waves from Extreme Mass Ratio Inspirals

Nicolás Yunes,[1,2] Bence Kocsis,[2] Abraham Loeb,[2] and Zoltán Haiman[3]

[1] *Dept. of Physics and MIT Kavli Institute, 77 Massachusetts Avenue, Cambridge, MA 02139.*
[2] *Harvard-Smithsonian Center for Astrophysics, 60 Garden St., Cambridge, MA 02138, USA.*
[3] *Department of Astronomy, Columbia University, 550 West 120th Street, New York, NY 10027*

(Dated: January 16, 2013)

We study the effects of a thin gaseous accretion disk on the inspiral of a stellar–mass black hole into a supermassive black hole. We construct a phenomenological angular momentum transport equation that reproduces known disk effects. Disk torques modify the gravitational wave phase evolution to detectable levels with LISA for reasonable disk parameters. The Fourier transform of disk-modified waveforms acquires a correction with a different frequency trend than post-Newtonian vacuum terms. Such inspirals could be used to detect accretion disks with LISA and to probe their physical parameters.

The inspiral of a stellar-mass compact object (SCO), such as a black hole or neutron star, into a supermassive black hole (SMBH) is among the most interesting gravitational wave (GW) sources for the Laser Interferometer Space Antenna (LISA) [1]. Extreme mass ratio inspirals (EMRIs) can be produced through fragmentation of accretion disks into massive stars [2, 3] or through capture of compact remnants by hydrodynamic drag [4], which are believed to be mass-segregated in galactic nuclei [5], as well as through other channels [6]. Stars which reside within an accretion disk will lead to EMRIs, provided they become a SCO in less time than their inward migration time. Although the expected EMRI event rate is rather uncertain (between a few tens to hundreds over LISA's lifetime, including coalescences and inspiral-only events [7]), a detectable fraction may originate in active galactic nuclei (AGNs) with an accretion disk.

Accretion disks are efficient at extracting orbital angular momentum from the extreme mass-ratio binary. The SCO torques the disk gravitationally, inducing spiral density waves that carry away angular momentum [8]. In planetary disks, the same phenomenon leads to *migration* of planets towards their parent star. Planetary migration has been classified into different types (determined by disk parameters, the EMRI's mass ratio and orbital separation) to distinguish circumstances where a gap opens around the planet (Type-II) from those without a gap (Type-I). In EMRIs, migration becomes the dominant source of angular momentum transport at separations $\gtrsim 100M_\bullet$, where $M_\bullet$ is the SMBH mass [3, 9] (we use units $G = c = 1$).

Migration changes the relation between the binary's binding energy and the GW luminosity, and hence it affects the inspiral rate and the GW phase evolution. EMRIs enter the LISA sensitivity band only inside $\lesssim 50M_\bullet$, where GW angular momentum transport is dominant. Thus, migration acts perturbatively in LISA EMRIs. In this Letter, we examine whether the imprint of migration on the EMRI GW observables is detectable by LISA. In a companion paper [10], we consider a broader range of disk effects and their impact on GWs in more detail.

Disk Properties and Migration.—We consider radiatively-efficient, geometrically thin accretion disks, whose two most important free parameters are the accretion rate $\dot{M}_\bullet$ (overhead dots denote time-derivatives) and the α-viscosity parameter. AGN observations suggest an accretion rate $\dot{M}_\bullet \equiv \dot{m}_\bullet \dot{M}_{\bullet\rm Edd} \in (0.1, 1)\dot{M}_{\bullet\rm Edd}$ [11]. Evidence for the magnitude of α is inconclusive, with plausible theoretical and observed ranges in $(0.01, 1)$ [12]. We focus on Shakura-Sunyaev α-disks [13] and β-disks [14], which differ in whether viscosity is proportional to the total pressure (gas plus radiation) or only the gas pressure, respectively. This affects the surface density ($\Sigma \propto r^{3/2}$ and $r^{-3/5}$ for α- and β-disks when opacity is dominated by electron scattering). The local disk mass is much larger for β–disks at radii $r \ll 10^3 M_\bullet$, leading to a stronger GW imprint.

In the absence of a gap, Type-I migration models for angular momentum transport have been formulated [15, 16] but they are very sensitive to opacity and radiation processes [17] and lack the stochastic features observed in magnetohydrodynamic simulations [18]. The presence of a gap leads to Type-II models for angular momentum exchange [19, 20]. These also oversimplify the process, assuming either a steady state or quasi-stationarity. Type-II migration can also cease interior to a decoupling radius, $r_{\rm d}$, in the late stages of the inspiral, when the gas accretion velocity outside the gap becomes slower than the SCO's GW-driven inspiral velocity [21]. Alternatively, the gap can refill by non-axisymmetric or 3D inflow, restoring viscous torque balance from inside and outside the SCO's orbit and slowing the gaseous migration [22]. Migration is mostly unexplored in the regime relevant to LISA EMRIs, i.e. for radiation-pressure dominated, optically-thick, geometrically-thin, relativistic, magnetized and turbulent disks, with the SCO's mass $m_\star$ exceeding the local disk mass.

Astrophysical uncertainties regarding accretion disks

		A_0	A_1	A_2	A_3	A_4	B
[16], Iα	●	7.2×10^{-19}	-1	-3	1	0	8
[16], Iβ	●	6.5×10^{-13}	$-4/5$	$-7/5$	6/5	0	59/10
[19], IIα	□	6.2×10^{-10}	0	1	3	-2	4
[19], IIβ	□	4.4×10^{-6}	1/2	5/8	13/8	$-11/8$	25/8
[20], IIβ	△	1.6×10^{-7}	2/7	11/14	31/14	$-23/14$	7/2

TABLE I. Disk parameters for Type I and II migration models in α and β disks.

and migration in the regime relevant to LISA EMRIs lead us to consider a general power-law relation,

$$\dot{\ell}_\star = \dot{\ell}_{\rm GW}\left(1+\delta\dot{\ell}\right), \tag{1}$$

$$\delta\dot{\ell} \equiv A\,\bar{r}^B = A_0\,\alpha_1^{A_1}\,\dot{m}_{\bullet1}^{A_2}\,M_{\bullet5}^{A_3}\,m_{\star1}^{A_4}\,\bar{r}^B, \tag{2}$$

where $\dot{\ell}_\star$ is the SCO's rate of change of specific angular momentum, $\dot{\ell}_{\rm GW}$ is the loss due to GWs, and $\delta\dot{\ell}$ a correction induced by migration. The power-law form in the reduced radius $\bar{r}\equiv r/M_\bullet$ involves an amplitude A, which is parameterized in terms of normalized accretion disk ($\alpha_1\equiv\alpha/0.1$, $\dot{m}_\bullet=\dot{m}_\bullet/0.1$), and mass parameters [$M_{\bullet5}=M_\bullet/(10^5\,{\rm M}_\odot)$, $m_{\star1}=m_\star/(10\,{\rm M}_\odot)$]. The power-law indices $(A_{i>0},B)$ are given in Table I for representative migration models: rows 1–2 correspond to Type I [16], 2–4 to steady state Type-II [19], 5 to quasistationary Type-II migration in the asymptotic limit for small $\bar{r}$ [20] (the latter is available for β–disks only). The gap decouples and Type-II migration ceases ($A\approx0$) interior to $\bar{r}_{\rm d}=1.4\times10^{-5}\alpha_1^{-2}\dot{m}_{\bullet1}^{-4}M_{\bullet5}^{-2}m_{\star1}^2\lambda^5$ for α and $15\,\alpha_1^{-4/13}\dot{m}_{\bullet1}^{-2/13}M_{\bullet5}^{-4/13}m_{\star1}^{5/13}\lambda^{2/13}$ for β disks, where λr is the gap radius (we adopt $\lambda=1.7$ [23]). Since disk effects become stronger at larger radii, $B>0$.

GW Implications.—The change in the angular momentum dissipation rate due to migration modifies the GW evolution, leading to a change in the accumulated GW phase and spectrum. For circular orbits, the quadrupolar GW phase can be computed from $\phi_{\rm GW}=2\int_{r_0'}^{r_f}dr\,\Omega\,\dot{\ell}_\star^{-1}\,d\ell/dr$, where the orbital frequency is $\Omega\simeq(M_\bullet/r^3)^{1/2}$, the binary's specific angular momentum is $\ell=r^2\Omega=M_\bullet^{1/2}r^{1/2}$, while the specific angular momentum flux $\dot{\ell}_\star$ is given by Eq. (1). For a fixed final EMRI separation r_f and observation time $T_{\rm obs}$, the initial separation r_0' is different from what it would be in vacuum, as the radial inspiral evolution $\dot{r}$ is determined by $\dot{\ell}_\star$: $r=\int_{r_0'}^{r_f}\dot{\ell}_\star(d\ell/dr)^{-1}dr$. For an unperturbed EMRI, $(\bar{r}_f/\bar{r}_0)^{-4}\approx1+33\,(m_{\star1}/M_{\bullet5}^2)(T_{\rm obs}/{\rm yr})(\bar{r}_f/10)^{-4}$.

The correction to the GW phase, $\delta\phi_{\rm GW}\equiv\phi_{\rm GW}-\phi_{\rm GW}^{\rm vac}$, where $\phi_{\rm GW}^{\rm vac}$ is the accumulated phase in vacuum, is then

$$\delta\phi_{\rm GW} = \bar{A}\,\frac{M_{\bullet5}}{m_{\star1}}\,\bar{r}_0^{B+5/2} \times\left(1+\frac{2B+5}{3}x^{B+4}-\frac{2B+8}{3}x^{B+5/2}\right), \tag{3}$$

where $\bar{A}\equiv-(3\times4^{-1/2}\times5^5)(4+B)^{-1}(5+2B)^{-1}A$, $x\equiv r_f/r_0$, $\bar{r}_0\equiv r_0/M_\bullet$ and we have expanded in $\delta\dot{\ell}\ll1$, which holds in the LISA regime. For fixed $T_{\rm obs}$, we find that $|\delta\phi_{\rm GW}|$ increases and decreases with $m_\star$ for the Type-I and II models of Table I, respectively.

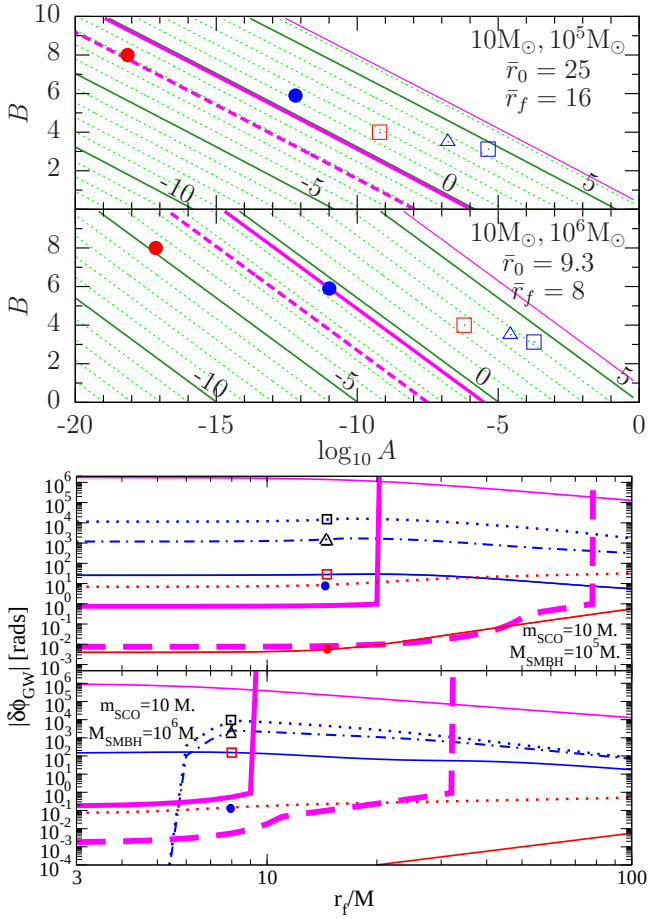

FIG. 1. Top: contours of $\log_{10}|\delta\phi_{\rm GW}|$ for different interaction models of two EMRI systems observed for one year. Bottom: $|\delta\phi_{\rm GW}|$ for different $\bar{r}_f$ for the 5 models in Table I. Many of the models – especially those resembling β-disks and Type II migration – shown in Table I (marked with symbols in the top, and individual curves on the bottom) lie well above the LISA sensitivity level (thick magenta lines).

The top panel of Fig. 1 plots the dephasing in Eq. (3) for two typical LISA EMRIs at fixed $r_f>r_{\rm d}$ as contours for different torque parameters (A,B). The specific migration models defined in Table I with $\alpha_1=1=\dot{m}_{\bullet1}$ are marked with symbols. The bottom panel shows $\delta\phi_{\rm GW}$ for those models but with different r_f, fixing $T_{\rm obs}=1\,{\rm yr}$ (c.f. LISA's planned lifetime is 3 years). For comparison, we also plot the total GW phase accumulation [$\mathcal{O}(10^6)$ top, thin line] and a rough measure of LISA's accuracy to phase measurements: $\delta\phi_{\rm GW}>10/\rho$, where ρ is the signal to noise ratio $\rho(h)=4\int_{r_0}^{r_f}{\rm d}r({\rm d}f/{\rm d}r)|\tilde{h}|^2S_n^{-1}[f(r)]$, with $S_n[f(r)]$ the LISA detector noise [24] and $\tilde{h}$ the Fourier transform of the orientation-averaged GW sig-

nal. We evaluate ρ at 1 Gpc (or redshift $z \approx 0.2$; thick solid line) and at 10 Mpc (or $z \approx 0.002$; thick dashed line). For $\rho < 10$, we assume the EMRI is not detected at all, which explains the sharp rise in the detection level beyond a certain r_f. Migration with a gap (empty symbols) causes a bigger phase shift because of the pileup of mass outside the gap. For $\bar{r}_{\rm d} \lesssim \bar{r}_f \lesssim 50$ but fixed $(A, B, M_\bullet, m_\star, T_{\rm obs})$, the phase shift is constant within a factor ~ 3, but it quickly drops off for the Type-II models interior to the gap decoupling radius $r_{\rm d}$ where $A \to 0$.

The Newtonian estimates presented here suggest that LISA EMRI observations might be able to probe accretion-disk induced migration. Figure 1 shows that a large sector of parameter space (A, B) exists where the dephasing is large enough to be detectable, and $\delta\phi_{\rm GW}$ is very sensitive to the disk model and its parameters. One might worry, however, that the estimates in Fig. 1 are inaccurate due to the use of a Newtonian waveform model. We have verified that this is not the case through a relativistic waveform model that employs the calibrated effective-one-body scheme [25]. We have generated 1 year-long waveforms for the systems plotted in Fig. 1 and included modifications to the radiation-reaction force due to migration, as parameterized by Eq. (2). Overall, we find the Newtonian results to be representative of the fully relativistic ones [10].

Just because migration produces a sufficiently large phase correction does not necessarily imply that LISA can measure it. For that to be possible, migration phase corrections must be non-degenerate, or at worst, weakly correlated with other system parameters. One can study if this is the case by computing the Fourier transform of the GW observable. We employ the stationary phase approximation (SPA) [26], where one assumes the GW phase varies much more rapidly than the amplitude. The Fourier transform of $h(t) = A(t)\exp[i\phi_{\rm GW}(t)]$ can then be approximated as $\tilde{h}(f) = \tilde{A}(f)\exp[i\psi(f)]$, where $\tilde{A}(f) \equiv (4/5)A[t(f)]\dot{f}^{-1/2}$ and $\psi(f) \equiv 2\pi f t_0 - \phi_{\rm GW}(t_0)$, where f is the GW frequency and t_0 is the stationary point, defined by $2\pi f = (d\phi_{\rm GW}/dt)_{t=t_0}$ [26].

The corrections due to migration on the Fourier transform of the GW phase in the SPA, $\delta\psi \equiv \psi - \psi_{\rm vac}$, are

$$\frac{\delta\psi}{\psi^{\rm Newt}_{\rm vac}} = \tilde{A}\,\bar{\eta}^{2B/5}\,\bar{u}^{-2B/3}\,, \qquad (4)$$

where we have defined $\tilde{A} \equiv -2^{2-8B/5}5^{1-8B/5}(4+B)^{-1}(5+2B)^{-1}A\exp(6.46B)$, the normalized symmetric mass ratio $\bar{\eta} \equiv m_{\star 1}/M_{\bullet 5}$ and $\bar{u} \equiv (\pi\mathcal{M}f)/(6.15\times10^{-5})$, and where $\mathcal{M} = m_\star^{3/5}M_\bullet^{2/5}$ is the chirp mass and $\psi^{\rm Newt}_{\rm vac} = (3/128)(\pi\mathcal{M}f)^{-5/3}$ is the leading-order (Newtonian) vacuum Fourier phase. The amplitude of the SPA Fourier transform is corrected in a similar fashion: $\delta|\tilde{h}|/|\tilde{h}|_{\rm vac} \sim \delta\psi/\psi_{\rm vac}$.

Equation (4) is to be compared with the intrinsic general relativity (GR) corrections to the vacuum Fourier GW phase: $\psi_{\rm vac}/\psi^{\rm Newt}_{\rm vac} = \sum_{n=0}^{\infty} a_n u^{2n/3}$, where $a_q = a_q(m_\star, M_\bullet)$, and the modulation induced by the orbital motion of LISA around the Sun. Migration corrections lead to negative frequency exponents in the Fourier phase (in Eq. (4), $-2B/3 < 0$), while GR, post-Newtonian corrections in vacuum lead to positive powers of frequency, while the detector orbit is periodic with a 1 yr period. For a sufficiently strong signal, this suggests it might be possible to separate the migration effects from the other GR and detector orbit induced phase corrections.

Modified gravity theories might introduce corrections similar to Eq. (4). The parameterized post-Einsteinian (ppE) framework [27], devised to search for generic GR deviations in GW data, postulated such a phase modification, allowing for both positive and negative B. Degeneracies between disk and modified gravity effects with negative frequency exponents ($B > 0$) could then exist (e.g. Brans-Dicke theory or $G(t)$ theories). The latter, however, have already been greatly constrained by binary pulsar observations [28]. Moreover, alternative theory modifications should be present in all EMRIs, while disk effects will be present in only a small subset.

A precise measure of whether a migration-modified waveform $\tilde{h}_1(f)$ is distinguishable from a vacuum waveform $\tilde{h}_2(f;\vec{\lambda})$, where $\vec{\lambda}$ stands for all disk parameters, requires a detailed Monte Carlo study that maps the likelihood surface. A rough measure of distinguishability can be obtained by calculating the signal-to-noise ratio (SNR) of the difference between a vacuum and a non-vacuum waveform $\rho(\delta h)$ by minimizing only over a time and a phase shift. Using this crude measure, we demonstrate in the bottom panel of Fig. 2 that most of the migration models of Table I lead to $\rho(\delta h) > 10$ within 4 months of observation for a source at 1 Gpc.

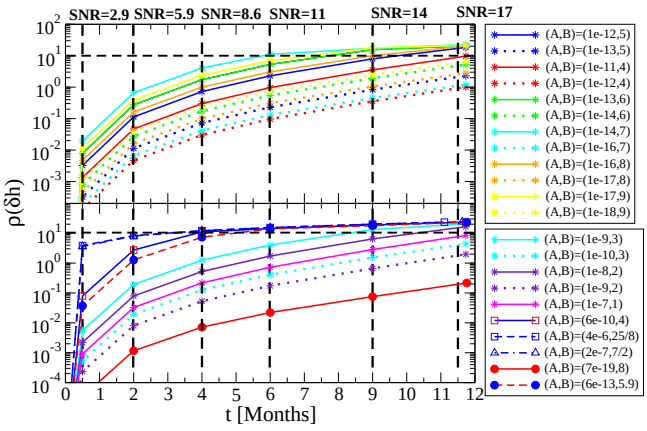

FIG. 2. $\rho(\delta h)$ as a function of observation time. Observe that $\rho(\delta h) > 5$ within 1 year for a large set of (A, B).

Going beyond Table I, there exists a large sector of disk parameter space (A, B) for which the SNR of the waveform difference exceeds threshold $\rho(\delta h) > 10$. Figure 2 plots $\rho(\delta h)$ at 1 Gpc as a function of observation time

for different values of (A, B) in Eq. (2). We also indicate (with labels over the vertical dashed lines) the SNR of the vacuum waveform at 1 Gpc and $T = (0.5, 2, 4, 6, 9, 11.5)$ months. We calculate the waveforms with the relativistic model of [25] and $(M_{\bullet 5}, m_{\star 1}) = (1, 1)$, SMBH spin angular momentum $|S_\bullet| = 0.9M_\bullet^2$ coaligned with the orbital angular momentum, and initial and final separations $(r_0, r_f) \sim (24.5, 16)M_\bullet$. Observe that for a large set of disk parameters (A, B), $\rho(\delta h) > 10$ within a one-year observation. Fitting to the smallest A with $\rho(\delta h) > 10$ for fixed B, we find that for these masses and orbital radii, LISA could measure $\log_{10} A \gtrsim a_1 + a_2 B$, with $a_1 = -5.7 \pm 0.4$ and $a_2 = -1.4 \pm 0.2$.

Discussion.—The GW observation of EMRI signals with LISA could be used to probe the uncertain physics of accretion disks. In particular, spiral density waves generated by an orbiting SCO can transfer sufficient orbital angular momentum to alter the GW signal at levels that are detectable by LISA. The effects are strongest for parameter choices resembling Type II migration (i.e. with the SCO opening a gap) in relatively massive β disks. A very crude (diagonal) Fisher analysis suggests that LISA could measure certain sectors of disk parameter space to better than 10%, for vacuum SNRs larger than 10, the details of which will be presented in a companion paper [10]. This is no surprise considering that $\delta\phi_{\rm GW}$ is at worst ~ 10 times higher than LISA's sensitive curve in Fig. 1. Detection of the predicted migration effect would reduce the uncertainty in existing theoretical models and offer the potential for extending the discussion to more complicated geometries (such as EMRIs with eccentric and/or inclined orbits).

The detection of EMRIs in AGNs and the extraction of disk-parameters improve the prospects for finding electromagnetic counterparts in the LISA error volume with consistent luminosities [29]. Coincident measurements would also allow EMRIs to serve as standard sirens to independently test cosmological models [30]. LISA EMRIs are low-redshift events, for which weak lensing errors, dominant in comparable mass, SMBH standard sirens at higher-z, are subdominant [29]. Disk effects will not compromise the ability to constrain cosmological parameters, as they enter the GW observable with a different frequency signature, and are thus weakly correlated. Migration effects may also deplete the unresolved low-frequency EMRIs that contribute to the GW confusion noise background [24].

Acknowledgements.—BK and NY acknowledge support from the NASA through Einstein Fellowship PF9-00063 and PF0-110080 issued by the Chandra X-ray Observatory, operated by the SAO, on behalf of NASA under NAS8-03060. AL acknowledges support from NSF grant AST-0907890 and NASA grants NNX08AL43G and NNA09DB30A, and ZH from the Polányi Program of the Hungarian National Office for Research and Technology (NKTH) and from NASA grant NNX08AH35G.

[1] LISA, `www.esa.int/science/lisa`.
[2] J. Goodman and J. C. Tan, ApJ **608**, 108 (2004).
[3] Y. Levin, Mon. Not. Roy. Astron. Soc. **374**, 515 (2007).
[4] L. Šubr and V. Karas, A&A **352**, 452 (1999); J. Miralda-Escudé and J. A. Kollmeier, ApJ **619**, 30 (2005).
[5] M. Freitag, P. Amaro-Seoane, and V. Kalogera, ApJ **649**, 91 (2006).
[6] P. Amaro-Seoane, J. R. Gair, M. Freitag, M. C. Miller, I. Mandel, C. J. Cutler, and S. Babak, Classical and Quantum Gravity **24**, 113 (2007).
[7] J. R. Gair, Class. Quant. Grav. **26**, 094034 (2009).
[8] P. J. Armitage, (2007); W. R. Ward, Icarus **126**, 261 (1997).
[9] V. Karas and L. Šubr, A&A **376**, 686 (2001).
[10] B. Kocsis, N. Yunes, and A. Loeb, In preparation (2011).
[11] J. A. Kollmeier et al., ApJ **648**, 128 (2006).
[12] M. E. Pessah, C. Chan, and D. Psaltis, ApJ **668**, L51 (2007); G. Dubus, J. Hameury, and J. Lasota, A&A **373**, 251 (2001); A. R. King, J. E. Pringle, and M. Livio, MNRAS **376**, 1740 (2007).
[13] N. I. Shakura and R. A. Sunyaev, Astron. Astroph. **24**, 337 (1973).
[14] P. J. Sakimoto and F. V. Coroniti, ApJ **247**, 19 (1981).
[15] P. Goldreich and S. Tremaine, ApJ **241**, 425 (1980).
[16] H. Tanaka, T. Takeuchi, and W. R. Ward, ApJ **565**, 1257 (2002).
[17] S. Paardekooper and G. Mellema, A&A **459**, L17 (2006).
[18] R. P. Nelson and J. C. B. Papaloizou, MNRAS **350**, 849 (2004); G. Laughlin, A. Steinacker, and F. C. Adams, ApJ **608**, 489 (2004).
[19] D. Syer and C. J. Clarke, MNRAS **277**, 758 (1995).
[20] P. B. Ivanov, J. C. B. Papaloizou, and A. G. Polnarev, MNRAS **307**, 79 (1999).
[21] M. Milosavljević and E. S. Phinney, ApJ **622**, L93 (2005); Z. Haiman, B. Kocsis, and K. Menou, ApJ **700**, 1952 (2009).
[22] P. Artymowicz and S. H. Lubow, ApJ **467**, L77+ (1996); A. I. MacFadyen and M. Milosavljević, ApJ **672**, 83 (2008); J. Cuadra, P. J. Armitage, R. D. Alexander, and M. C. Begelman, MNRAS **393**, 1423 (2009).
[23] P. Artymowicz and S. H. Lubow, ApJ **421**, 651 (1994).
[24] L. Barack and C. Cutler, Phys. Rev. D **70**, 122002 (2004).
[25] N. Yunes, A. Buonanno, S. A. Hughes, M. C. Miller, and Y. Pan, Physical Review Letters **104**, 091102 (2010); N. Yunes, GW Notes, Vol. 2, p. 3-47 **2**, 3 (2009); N. Yunes, A. Buonanno, S. A. Hughes, Y. Pan, E. Barausse, *et al.*, (2010).
[26] E. Poisson and C. M. Will, Phys. Rev. D **52**, 848 (1995); N. Yunes, K. Arun, E. Berti, and C. M. Will, Phys.Rev. **D80**, 084001 (2009).
[27] N. Yunes and F. Pretorius, Phys.Rev. **D80**, 122003 (2009).
[28] N. Yunes, F. Pretorius, and D. Spergel, Phys.Rev. **D81**, 064018 (2010).
[29] B. Kocsis, Z. Frei, Z. Haiman, and K. Menou, ApJ **637**, 27 (2006); B. Kocsis, Z. Haiman, and K. Menou, ApJ **684**, 870 (2008).
[30] B. F. Schutz, Nature **323**, 310 (1986); D. E. Holz and S. A. Hughes, ApJ **629**, 15 (2005).